Arteriolar niches maintain haematopoietic stem cell quiescence

Yuya Kunisaki[1,2], **Ingmar Bruns**[1,2,6,*], **Christoph Scheiermann**[1,2,7,*], **Jalal Ahmed**[1,8,*], **Sandra Pinho**[1,2], **Dachuan Zhang**[1,2], **Toshihide Mizoguchi**[1,2], **Qiaozhi Wei**[1,2], **Daniel Lucas**[1,3], **Keisuke Ito**[1,2,3], **Jessica C. Mar**[4,5], **Aviv Bergman**[4], and **Paul S. Frenette**[1,2,3]

[1]Ruth L. and David S. Gottesman Institute for Stem Cell and Regenerative Medicine Research, Albert Einstein College of Medicine, Bronx, NY 10461, USA.

[2]Department of Cell Biology, Albert Einstein College of Medicine, Bronx, NY 10461, USA.

[3]Department of Medicine, Albert Einstein College of Medicine, Bronx, NY 10461, USA.

[4]Department of Systems and Computational Biology, Albert Einstein College of Medicine, Bronx, NY 10461, USA.

[5]Department of Epidemiology and Population, Health, Albert Einstein College of Medicine, Bronx, NY 10461, USA.

[6]Department of Hematology, Oncology and Clinical Immunology, Heinrich-Heine-University, Düsseldorf 40225, Germany.

[8]Mount Sinai School of Medicine, New York, NY 10029, USA.

Abstract

Cell cycle quiescence is a critical feature contributing to haematopoietic stem cell (HSC) maintenance. Although various candidate stromal cells have been identified as potential HSC niches, the spatial localization of quiescent HSCs in the bone marrow (BM) remains unclear. Here, using a novel approach that combines whole-mount confocal immunofluorescence imaging techniques and computational modelling to analyse significant tridimensional associations among vascular structures, stromal cells and HSCs, we show that quiescent HSCs associate specifically

Supplementary Information is linked to the online version of the paper at www.nature.com/nature.

Readers are welcome to comment on the online version of the paper.

with small arterioles that are preferentially found in endosteal BM. These arterioles are ensheathed exclusively by rare NG2^{+} pericytes, distinct from sinusoid-associated LepR^{+} cells. Pharmacological or genetic activation of HSC cell cycle alters the distribution of HSCs from NG2^{+} peri-arteriolar niches to LepR[+] peri-sinusoidal niches. Conditional depletion of NG2^{+} cells induces HSC cycling and reduces functional long-term repopulating HSCs in BM. These results thus indicate that arteriolar niches are indispensable to maintain HSC quiescence.

Somatic stem cells self-renew to maintain tissue homeostasis for the lifetime of organisms through tightly controlled proliferation and differentiation[1–3]. In the bone marrow (BM), recent studies have highlighted the critical influence of the microenvironment in regulating haematopoietic stem cell (HSC) maintenance[4]. Deletion `of genes involved in maintaining cell cycle quiescence has taught that unchecked HSC proliferation often leads to stem cell exhaustion[5–8]. While most HSCs are quiescent under homeostasis[9], they can undergo activation for example by interferon-mediated signals[7,10,11]. This raises the question of whether quiescent and proliferative HSCs are found in the same niche.

The identification of cellular constituents of the HSC niche has recently been the subject of intense studies. Initial reports have suggested that osteoblasts are niche cells as HSCs tend to localize near endosteal surfaces[12] and that factors increasing osteoblast numbers can also increase the number of HSCs[12,13]. N-cadherin[+] osteoblasts have been proposed to promote HSC quiescence via direct contact[12,14] and secretion of angiopoietin-1[15] or osteopontin[16,17]. However, the synthesis of these factors is not specific to osteoblasts and other studies have found that most BM HSCs are found near sinusoidal endothelial cells[18], and perivascular stromal cells including, CXCL12-abundant reticular (CAR) cells[19,20], Nestin[+] mesenchymal stem cells[21] or Leptin receptor (LepR)[+] cells[22]. Based on these data, a prevalent unifying interpretation of the literature has been that the osteoblastic and vascular niches confer distinct microenvironments promoting quiescence and proliferation, respectively[2,23]. However, this popular concept has not been supported by rigorous analyses. To evaluate this issue, we have used novel tridimensional (3D) BM imaging combined with computational modelling to assess significant relationships between endogenous quiescent HSCs and stromal structures. These studies have allowed us to identify distinct vascular niches mediating stem cell quiescence and proliferation.

HSCs significantly associate with bone marrow arterioles

To gain detailed insight into the 3D structure of the HSC niche, we prepared whole-mount tissues to visualise by confocal immunofluorescence imaging the architecture of long-bone and sternal marrow over ~75μm thickness (Fig. 1a,b and Extended Data Fig. 1a,b). To specifically label BM endothelial cells, we performed *in vivo* staining (Extended Data Fig. 1c–e). Whole-mount assessment of the femoral BM vasculature revealed an even distribution of the sinusoidal network that occupies 30±5% of the BM volume (Fig. 1c,d) and where individual sinusoidal vessels are regularly spaced by 46±1μm (Extended Data Fig. 1f). In addition to the sinusoidal network, 3D visualisation of the BM vasculature highlighted the presence of small calibre (10–20μm) Sca-1^{hi} VEGFR2^{+} VEGFR3^{−} arterioles[24], which were found predominantly in close proximity to the bone[25] and comprised a much smaller volumetric fraction 1.2 ± 0.1% of the BM (Fig. 1a–d and

Extended Data Fig. 2a,b). The vessels were confirmed as *bona fide* arterioles by their pronounced Tie-2-GFP expression[26], absence of *in vivo* staining with the sinusoid-specific Dil-Ac-LDL[26], and strong staining with the artery-specific dye Alexa Fluor633 (ref.[27]) (Fig. 1e and Extended Data Fig. 2b–f). The distribution of phenotypic CD150$^+$ CD48$^-$ CD41$^-$ Lineage$^-$ HSCs[18] was not uniform as they localized predominantly to the peripheral zone rather than in close proximity to the central vein in the long-bone BM (Fig. 1d and Extended Data Fig. 3a). We validated the identification of rare phenotypic HSCs by using whole-mount preparations of the mouse sternum[28]. Unlike long bones which are mostly occupied by adipocytes in adult humans[29], the sternum exhibits rich hematopoietic activity in both species. The mouse sternum is made of six thin bone compartments in which all HSCs can be enumerated (Fig. 1f and Extended Data Fig. 3b,c).

The absolute numbers of HSCs per sternal bone compartment, determined by whole-mount imaging, was similar to assessment by FACS, indicating that the staining of endogenous HSCs was reliable (Extended Data Fig. 3d). We next examined the spatial relationships between individual HSC and arterioles and sinusoids, by whole-mount immunostaining of sternal BM. We found that 36.8±1.8% and 67.1±3.5% of HSCs were located within 20μm distance from arterioles and sinusoids, and 14.9±2.5% and 32.9±5.2% were adjacent to those vessels, respectively (Fig. 1g,h and Extended Data Fig. 3e,f). The high proportion of HSCs near sinusoids is consistent with previous reports[18,19].

Since the BM sinusoidal network was dense and appeared to be regularly interspaced, we evaluated in more detail whether the spatial distribution of HSCs was independent of the sinusoidal network or significantly biased in relation to a putative sinusoidal niche. To address this issue, we developed a computational simulation to assess the statistical relevance of these associations (Extended Data Fig. 4a–c). We carried out 1,000 simulations in which 20 HSCs were randomly positioned on images of whole-mount prepared sterna. We found that the mean distance observed *in situ* to sinusoids could not be statistically differentiated from that of randomly placed HSCs (14.2μm and 14.8μm for random and observed; Fig. 1i). By contrast, the observed mean distance to arterioles (52.0μm) was highly statistically different from that of randomly placed HSCs (78.3μm, P = 0.012; Fig. 1i). Thus, these data suggest that associations between HSCs and arterioles are highly significant whereas the close relationship observed with sinusoids could not be discriminated from that of a random distribution.

Distinct Nestin$^+$ cells segregate with distinct blood vessels

Nestin$^+$ perivascular cells have been identified as HSC niche cells containing all BM mesenchymal stem cell activity[21]. Detailed 3D imaging and FACS analyses revealed two distinct types of Nes-GFP$^+$ cells in the BM based on their GFP expression levels and cellular morphology (Fig. 2a,b and Extended Data Fig. 5a). Nes-GFP^{bright} cells were much rarer (~0.002% of BM) than Nes-GFP^{dim} cells (Fig. 2a and Extended Data Fig. 5b), and found exclusively along arterioles in both sternal and long-bone BM (Extended Data Fig. 2d,e, 5c–h). Consistent with this observation, similar HSC distribution patterns were obtained when plotting distances from arterioles or from Nes-GFP^{bright} cells (hereafter referred to as peri-arteriolar Nestin cells, Nes^{peri}; Fig. 1g,h and Extended Data Fig. 3e,f, P = 0.97). The more

abundant Nestin-GFP^{dim} population was reticular in shape (hereafter referred to as Nes^{retic} cells) and was largely associated with sinusoids (Fig. 2b and Extended Data Fig. 3e,f, 5g). Nes^{peri} cells, but not Nes^{retic} cells, were decorated with tyrosine hydroxylase (TH)$^+$ sympathetic nerves and glial fibrillary acidic protein (GFAP)$^+$ Schwann cells which were reported to modulate HSC behaviour in the BM[30–32] (Fig. 2c and Extended Data Fig. 5i). While both Nestin$^+$ cell subsets accounted for the mesenchymal progenitor activity (CFU-F) in BM, most CFU-F were contained in Nes^{peri} cells (Extended Data Fig. 5j). To get additional insight into potential differences between these two stromal subsets, we subjected Nes^{peri} and Nes^{retic} cells to RNA-seq analyses. Comparison of the whole genome transcriptome revealed differential enrichment of several molecular pathways and functional clusters, including HSC niche, cytokine/receptor interactions, DNA replication and cell cycle (Fig. 2d,e and Supplementary Table 1). Indeed, Nes^{peri} cells showed significantly higher expression of genes associated with the HSC niche (Fig. 2d,e and Extended Data Fig. 5k). In addition, expression of genes in two pathways, DNA replication and cell cycle, was significantly enriched in Nes^{retic} cells (Fig. 2d,e), suggesting that the two subsets had differing cell cycle characteristics.

Arteriolar Nes^{peri} niche cells are quiescent and protected from myeloablation

Based on these results, we evaluated in more detail the cell cycle status of BM stromal cells, and more specifically of Nes^{retic} and Nes^{peri} cells. Expression of the nuclear proliferation markers, Ki-67 and proliferation cell nuclear antigen (PCNA), in Nes^{peri} cells was significantly lower than in Nes^{retic} cells and CD45$^-$ Ter119$^-$ CD31$^-$ Nes-GFP$^-$ stromal cells (Fig. 3a,b), which was confirmed by FACS analysis (Fig. 3c,d). To test the relevance of niche cell quiescence, we challenged mice with 5-fluorouracil (5FU), a drug that kills cycling cells. After 5FU administration, Nes^{peri} cells were largely preserved structurally and numerically compared to Nes^{retic} cells (Fig. 3e–g), confirming their quiescent state.

HSC quiescence is associated with localization in vascular niches

We hypothesized that the arteriolar quiescent niche cells may themselves harbour quiescent HSCs. Consistent with previous studies[10,33], we found that most HSCs were not actively cycling, but ~20% of HSCs were in the non-quiescent G1 phase of the cell cycle (Extended Data Fig. 6a). Prolonged quiescence has been referred to as dormancy and tracked as label-retaining cells (LRCs)[10]. We first evaluated the spatial associations of dormant HSCs with Nes^{peri} cells by LRC pulse-chase experiments with EdU in the long-bone BM. Significantly more EdU$^+$ CD150$^+$ CD48$^-$ CD41$^-$ Lineage$^-$ HSCs compared to total HSCs were located within 20μm distance from Nes^{peri} cells (Fig. 4a,b and Extended Data Fig. 6b; 65.8±0.8% vs 44.3±1.8%, P = 0.016). We next analysed the cell cycle status and distribution of HSCs in relation to arterioles with Ki-67 staining in the sternal BM and found that a significantly higher proportion of Ki-67$^-$ quiescent HSCs were located within 20μm distance compared to Ki-67$^+$ non-quiescent HSCs (Fig. 4c,d,g and Extended Data Fig. 6c,d). There was no significant difference in the proportions of adjacent cells between quiescent and non-quiescent HSCs (Extended Data Fig. 6b,c), suggesting that proximity to arterioles, rather than direct contact, promotes HSC quiescence. Since osteoblasts have been suggested to be

associated with quiescent HSCs[12,14–17], we evaluated the distribution of HSCs in relation to osteoblasts in the sternal BM using transgenic mice expressing GFP under a 2.3kb fragment of the collagen promoter (Col2.3-GFP), in which osteoblasts and osteocytes express GFP[34]. We found that 20.7±1.9% of total HSCs were located within 20μm distance from Col2.3-GFP+ cells (Fig. 4e and Extended Data Fig. 6e). We performed the computational simulation with Col2.3-GFP+ cells and found that in contrast to arterioles, HSCs were not significantly associated with Col2.3-GFP+ cells (Extended Data Fig. 6f). Moreover, there was no significant difference in the distribution of quiescent and non-quiescent HSCs in relation to Col2.3-GFP+ cells in the sternal BM (Fig. 4f,g and Extended Data Fig. 6g, P = 0.93). These results suggest that quiescent HSCs are preferentially associated with arterioles in both long-bone and sternal marrow.

To test this idea using functional assays, we evaluated HSC-arteriole associations in mice treated with 5FU. We found that at nadir, on days 3 and 7, the vast majority of HSCs was closely associated with Nes^{peri} cells (Control/Day 3/Day 7; 34.4±1.0/71.1±3.9/70.6±4.0% in 0–20μm) and that HSCs expanded in further distance from Nes^{peri} cells upon recovery in the sternal BM (Fig. 4h and Extended Data Fig. 6h,i). These data indicate that arterioles indeed provide a milieu promoting quiescence for both HSCs and their niche cells, and a safe harbour to protect them against genotoxic insults.

We next tested whether changes in HSC cycling would lead to altered distribution. To this end, we injected mice with polyinosinic-polycytidylic acid (Poly(I:C)), a compound reported to induce proliferation of HSCs via interferon-α (IFN–α) production, which can lead to HSC exhaustion[7,8]. Poly(I:C) treatment increased the fraction of non-quiescent HSCs (Extended Data Fig. 7a) and altered their distribution in relation to arterioles in that the percentage of HSCs within 20μm was significantly reduced compared to PBS-treated animals in the sternal BM (Extended Data Fig. 7b, P = 0.007). Furthermore, we evaluated a genetic mouse model deficient in promyelocytic leukaemia protein (*Pml*$^{−/−}$) that was shown to compromise HSC quiescence in a cell-autonomous manner and caused HSC exhaustion[6]. Remarkably, endogenous HSCs were distributed significantly further away from arterioles in *Pml*$^{−/−}$ mice compared to wild type (WT) animals (Extended Data Fig. 7c, P=1.9×10$^{−6}$). Notably, the location of quiescent Ki-67$^{−}$ cells was dramatically affected (Extended Data Fig. 7d,e). These data suggest the possibility that there are spatially distinct niches for quiescent and proliferating HSCs in the BM.

To further confirm this notion, we treated mice with granulocyte colony-stimulating factor (G-CSF), a drug commonly used to mobilise HSCs from the BM to the circulation, and that is also known to induce HSC proliferation[35,36]. Short-term (1 or 2 days) administration of G-CSF led to altered HSC distribution further away from Nes^{peri} cells. By contrast, further treatment (4 days) led to expansion of HSCs around Nes^{peri} cells (Extended Data Fig. 7f,g). In line with these data, G-CSF also down-regulated HSC retention factors such as CXCL12 in the Nestin+ niche cells[21], which also may contribute to the shift from the quiescent to the proliferative (mobilisable) niches at early phase, the release of the mobilisable pool, and HSC replenishment at late phase. This model further highlights the importance of local cues in fine-tuning HSC behaviour in the BM.

NG2⁺ Nes-GFP^bright periarteriolar niche cells promote HSC quiescence

LepR⁺ perivascular cells have been reported to represent an important source of stem cell factor (SCF) required for the maintenance of HSCs in the BM[22]. Since Nestin⁺ cells were shown to express large amounts of *Scf*[21], we evaluated the overlap between Nes^peri or Nes^retic cells and LepR⁺ cells. Using triple-transgenic *Lepr-cre/loxp*-Tomato/Nes-GFP mice, we found that LepR⁺ cells were adjacent to sinusoids in a manner similar to Nes^retic cells (Extended Data Fig. 8a). Indeed, Nes^retic cells largely overlapped (~80%) with LepR⁺ cells whereas we found no overlap between Nes^peri and LepR⁺ cells (Extended Data Fig. 8b,c). By contrast, Nes^peri cells, but not Nes^retic, were positive for the classical pericyte marker NG2 (chondroitin sulphate proteoglycan-4, Cspg4) and α-smooth muscle actin (αSMA)[37] (Extended Data Fig. 9a–f). To examine further the expression of NG2 on Nes^peri cells, we generated triple-transgenic mice to label both NG2⁺ and Nestin⁺ cells (NG2-*cre*^ERTM/*loxp*-Tomato/Nes-GFP mice). In these mice, 30% of Nes^peri cells were labelled by the NG2-*cre*^ERTM transgene (Fig. 5a,b and Extended Data Fig. 9g,h), a recombination efficiency consistent with that reported for oligodendrocyte progenitors in the brain[38]. Notably, no labelling was observed in Nes^retic cells or in other stromal cells (Fig. 5b and Extended Data Fig. 9i).

To examine the function of NG2⁺ Nes^peri cells in HSC maintenance, we intercrossed NG2-*cre*^ERTM with an inducible diphtheria toxin receptor (iDTR) line. Tamoxifen and diphtheria toxin (DT) treatment depleted ~55% of Nes^peri cells without significantly affecting the vascular volume as determined by whole-mount imaging 7–16 days after DT administration (Fig. 5c and Extended Data Fig. 10a–c). NG2⁺ cell depletion also did not affect the expression of HSC niche genes in endothelial cells (Extended Data Fig. 10d,e). However, depletion of NG2⁺ cells altered HSC localization away from arterioles (Fig. 5d and Extended Data Fig. 10f) and switched them into non-quiescent status (Fig. 5e,f). In addition, we found that the number and frequency of HSCs in the BM and spleen, as determined phenotypically (Fig. 5g and Extended Data Fig. 10g) and functionally using long-term culture-initiating cell (LTC-IC; Extended Data Fig. 10h,i) or competitive reconstitution assays (Fig. 5h), were significantly reduced 16 days after DT administration. These results indicate that depletion of NG2⁺ cells reduces the HSC pool rather than inducing mobilisation to extramedullary sites (Extended Data Fig. 10j). Taken together, these data strongly suggest that rare NG2⁺ periarteriolar cells promote HSC quiescence and are essential for HSC maintenance in the BM.

Discussion

Here, we show that arterioles organise a critical niche that maintains HSC quiescence in the BM. Arterioles are associated with both quiescent NG2⁺ niche cells and HSCs, suggesting that the vessel itself may be a critical gatekeeper of stem cell quiescence in the BM. Arterioles are structurally distinct from sinusoids as they are surrounded by sympathetic nerves, layers of smooth muscle cells and matrix components to carry blood from the heart under high pressure (Supplementary Table 2). These differing characteristics translate into significant differences in the transcriptional program of arteriolar and venular endothelial cells[39]. Likewise, arteriolar Nes^peri cells and sinusoidal Nes^retic cells can be distinguished by

their individual transcriptional profiles reflecting relative enrichments in cell cycle quiescence and HSC niche-related genes in Nes[peri] cells. The present data show that upon severe genotoxic insult, the mitotically active Nes[retic] sinusoidal niche cells are largely destroyed, whereas that quiescent Nes[peri] arteriolar niche cells are chemoresistant. The association and quiescence of both haematopoietic and mesenchymal stem cells at this site may thus endow arterioles with the potential for orchestrating haematopoietic and stromal regeneration[40].

Given the recent studies showing that CXCL12 derived from mesenchymal progenitors marked by *Prx1-cre* contributes to HSC maintenance[41,42], it is possible that NG2+ Nes[peri] cells are also targeted by *Prx1-cre*. Although Nestin-GFP+ cells express high levels of *Scf*[21], Nes-*cre* mediated deletion of *Scf* has no effect on HSC function[22]. This may be due to the low recombination efficiencies among Nestin-GFP+ cells in this model, allowing for compensation by the non-targeted cells. In keeping with the notion that multiple niche constituents exert distinct functions, conditional deletion of *Cxcl12* by *Lepr-cre* does not affect HSC number in the BM, but induces their mobilization[42].

The idea that sinusoids may represent a proliferative niche is consistent with recent studies indicating that E-selectin, an adhesion molecule constitutively expressed in certain BM sinusoid microdomains[43], promotes HSC proliferation and blockade of E-selectin protects HSCs following chemotherapy or γ-irradiation[44]. It is therefore conceivable that a continuous exchange between the sinusoidal and arterial niches contributes to maintain a tightly controlled balance of HSC pool between proliferation and dormancy.

An arteriolar niche maintaining stem cell dormancy has the potential to protect haematopoietic malignancies and metastatic cancer stem cells. Gaining knowledge on the reciprocal regulation and functional correlation of these niches will thus have important implications in understanding stem cell fate in health and cancer.

Methods (online-only)

Animals

B6.Cg-Tg(Cspg4-cre/Esr1*)BAkik/J, STOCK Tg (TIE2GFP) 287Sato/J (Tie2-GFP) mice, C57BL/6-Gt(ROSA)26 Sortm1(HBEGF) Awai/J, B6.Cg-*Gt(ROSA)26Sortm14(CAG-tdTomato)Hze*/J, B6.129-*Leprtm2(cre)Rck*/J (*Lepr*-Cre) (all from Jackson laboratory), C57BL/6-CD45.1/2 congenic strains (from the National Cancer Institute), *Pml*^{−/−} mice (gift from P.P. Pandolfi) and Nes-GFP mice[45] were bred in our facilities. Col2.3-GFP mice were a gift from D.W. Rowe. All mice were maintained on the C57Bl6/J background. Unless indicated otherwise, 7–12 week-old male and female mice were used. No randomization or blinding was used to allocate experimental groups. All experimental procedures were approved by the Animal Care and Use Committees of Albert Einstein College of Medicine.

Immunofluorescence imaging

***In vivo* staining of BM endothelial cells—**To stain specifically endothelial cells, fluorescently conjugated antibodies (2 µg/mouse), AlexaFluor633(50 µg/mouse) or Dil-Ac-LDL (1 µg/g) were i.v. injected. Mice were perfused with PBS, 10 min (for antibodies) or 4

hours (for AlexaFluor633 and Dil-Ac-LDL) after injection to remove unbound reagents. Sterna and long bones were harvested for FACS or immunofluorescence imaging.

Preparations of whole-mount tissues and frozen sections of long bones— Femoral or tibial bones were perfusion-fixed and then post-fixed for 30 min in 4% paraformaldehyde (PFA), incubated in 15% and 30% sucrose for cryoprotection and embedded in OCT at −20°C. For whole-mount staining, bones were shaved on a cryostat until the BM cavity was fully exposed. Bones were carefully harvested from melting OCT. Frozen sections were prepared according to the Kawamoto method[46].

Whole-mount tissue preparation of the sternum—Sternal bones were harvested, transected with a surgical blade into 2–3 fragments. The fragments were bisected sagittally for the bone marrow cavity to be exposed, fixed in 4% PFA.

Immunofluorescence staining of whole-mount tissues and frozen sections of the sterna and long bones—Whole-mount tissues and sections were blocked / permeabilized in PBS containing 20% normal goat serum and 0.5% Triton X-100, and stained with primary antibodies for 1–3 days. The tissues were incubated with secondary antibodies for 2 hours. Images were acquired using a ZEISS AXIO examiner D1 microscope (Zeiss) with a confocal scanner unit, CSUX1CU (Yokogawa) and reconstructed in 3-D with Slide Book software (Intelligent Imaging Innovations) or Volocity software (PerkinElmer).

High-speed multichannel fluorescence intravital microscopy (MFIM)—We performed MFIM of the calvarial BM as previously described[47]. BM sinusoids and arterioles were visualized by administration of 10 μg of Rhodamine6G (R6G) and 50 μg of Alexa Fluor633, respectively.

Cell sorting and flow cytometry

For sorting of Nes[peri] and Nes[retic] cells, BM cells from 3–5 mice were pooled for a single experiment. BM cells were flushed and digested with 1mg/ml collagenase IV (Sigma) and 2mg/ml dispase (Gibco) in HBSS (Gibco) for 45 min at 37°C. All cell sorting experiments were performed using an Aria Cell Sorter (BD). Flow cytometric analyses were carried out using an LSRII flow cytometer equipped with FACS Diva 6.1 software (all BD). Dead cells and debris were excluded by FSC, SSC and DAPI (4',6-diamino-2-phenylindole) (Sigma) staining profiles. Data were analysed with FlowJo (Tree Star) or FACS Diva 6.1 software.

Antibodies and staining reagents

APC-anti-Gr-1 (RB6-8C5), PE-anti-CD11b (M1/70), biotin-anti-Lineage (TER-119, RB6-8C5, RA3-6B2, M1/70, 145-2C11), FITC/PE-anti-CD45.2 (104), PE/PE-Cy7-anti-Ly6A/E (D7), PE/PE-Cy7-anti-CD117 (2B8), biotin-anti-CD48 (HM48-1), biotin-anti-CD41 (MWReg30), FITC/PE/Alexa647-anti-Ki67 (SolA 15), biotin-anti-VEGFR3 (AFL4) (all from eBioscience), Alexa647-anti-VE-cadherin (BV13) APC-anti-CD31 (MEC13.3), FITC/PE/PE-Cy7-anti-CD45.1 (A20), PE-anti-CD150 (TC15-12F12.2) (all from Biolegend), PE-anti-Flk1 (Avas 12alpha1) (from BD Biosciences), anti-tyrosine hydroxylase and anti-NG2 (all from Millipore), anti-GFAP (DAKO), rabbit anti-GFP,

AlexaFluor488/568-anti-rabbit, AlexaFluor633 hydrazide and Dil-labelled acethylated low-density lipoprotein (Dil-Ac-LDL) (all from Invitrogen), Cy3-anti-αSMA antibody, Hoechst 33342, Rhodamine6G (R6G) (all from Sigma), were used in this study.

RNA isolation and quantitative real-time PCR (Q-PCR)

BM cells were harvested from Nes-GFP mice and Nes[peri] and Nes[retic] cells were sorted according to their specific flow cytometric profiles. mRNA was purified with polyT conjugated Dynabeads (Invitrogen) and conventional reverse transcription, using the Sprint PowerScript reverse transcriptase (Clontech), was performed in accordance with the manufacturer's protocol. Q-PCR was performed with SYBR Green (Roche) on an ABI PRISM 7900HT Sequence Detection System (Applied Biosystems). A primer concentration of 300 nM was found to be optimal in all cases. The sequences of the oligonucleotides used are included in Supplementary Table 3. The PCR protocol consisted of one cycle at 95 °C (10 min) followed by 40 cycles of 95 °C (15 s) and 60 °C (1 min). Expression of glyceraldehyde-3-phosphate dehydrogenase (*Gapdh*) was used as standards. The average threshold cycle number (C_t) for each tested mRNA was used to quantify the relative expression of each gene; $2^{-[Ct(gene) - Ct(standard)]}$.

RNA preparation and next-generation sequencing

Total RNA from sorted Nes[peri] and Nes[retic] cells was extracted using the RNAqueous kit (Life Technologies, Grand Island, NY USA) and concentrated using RNA Clean and Concentrator columns (Zymo Research Corporation, Irvine, CA USA). The integrity and purity of total RNA were assessed using an Agilent Bioanalyzer and OD260/280. cDNA was generated using a Clontech SMARTer Ultra Low RNA kit for Illumina Sequencing (Clontech Laboratories, Inc., Mountain View, CA USA) from 100pg–1ng of total RNA. cDNA was fragmented using Covaris (Covaris, Inc., Woburn, MA USA), profiled using an Agilent Bioanalyzer, and subjected to Illumina library preparation using NEBNext reagents (New England Biolabs, Ipswich, MA USA, catalog# E6040). The quality and quantity and the size distribution of the Illumina libraries were determined by an Agilent Bioanalyzer 2100. The libraries were then submitted for Illumina HiSeq2000 sequencing according to the standard operation procedure. Paired-end 90 or 100 nucleotide (nt) reads were generated and checked for data quality using FASTQC (Babraham Institute, Cambridge, UK) and subjected to data analysis using the platform provided by DNAnexus (DNAnexus, Inc, Mountain View, CA USA). For sorting of Nes[peri] and Nes[retic] cells, BM cells from 5–7 mice were pooled to get a single biological sample. Triplicate biological samples per population from three independent sortings were processed for RNA-seq.

RNA-sequencing (RNA-seq) data analysis

Pre-processing of the RNA-seq reads was performed by Otogenetic corporation. The RNA-seq reads were aligned using TopHat (version 1.3.3) and levels of gene expression were quantified using Cufflinks (version 1.3.0). Genes that did not pass the quantification status flagged by Cufflinks in either Nes[retic] or Nes[peri] cell populations were excluded from the analysis. The quantification status represents the success of the Cufflinks algorithm in quantifying expression from the RNA-seq reads that were mapped for a gene. Using

Bioconductor, genes were mapped to their Entrez Gene identifiers using the org.Mm.eg.db (version 2.5.0) package and to corresponding pathways based on definitions provided by the Kyoto Encyclopedia of Genes and Genomes (KEGG) via the KEGG.db (version 2.5.0) annotation package. The expression data was transformed by applying a $\log_2$-transformation to the ratio of (1+Nes^{peri} FPKM values) to (1+Nes^{retic} FPKM values) where the constant value of 1 was added because of the frequency of zero values observed in raw data. Log fold change of Nes^{peri}/Nes^{retic} expression was calculated for pathways defined by the KEGG orthology system (http://www.genome.jp/kegg-bin/get_htext?ko00001.keg) and using the HSC niche gene set defined by previous microarray studies[21,22]. Pathway enrichment of genes showing differential expression between Nes^{peri} and Nes^{retic} cells was assessed using a Kolmogorov-Smirnov test. P-values were adjusted for multiple testing using the Benjamini-Hochberg method which controls the false discovery rate.

EdU treatment and label-retaining assay

In vivo 5-ethynyl-2'-deoxyuridine (EdU, Invitrogen) labelling was performed as previously described with BrdU[10]. Briefly, Nes-GFP mice were pulsed with 1mg of EdU for 14 days followed by an EdU-free chase period of 90 days. Long bones were harvested and prepared for immunostaining. The frozen BM sections were stained with a Click-iT EdU Imaging Kit (Invitrogen) according to the manufacturer's instructions.

Cell cycle analysis

Cell cycle analysis was performed as previously described[10]. Briefly, BM cells were stained with surface markers, fixed in 2% paraformaldehyde in PBS, washed, permeabilized with 0.1% TritonX in PBS, and stained with anti-Ki67 antibody and Hoechst 33342 at 20 µg/mL for 30 min. After washing, cells were analysed by LSRII Flow Cytometer (Becton Dickinson).

CFU-F assay

Sorted cells ($1-3\times10^2$) were seeded per well in a 12-well adherent tissue culture plate using phenol-red free α-MEM (Gibco) supplemented with 20% FBS (Hyclone), 10% MesenCult stimulatory supplement (StemCell Technologies) and 0.5% penicillin-streptomycin. One-half of the media was replaced after 7 days and at day 14 cells were stained with Giemsa staining solution (EMD Chemicals).

In vivo treatments

PolyIC (5mg/kg) was injected i.p. every other day (2 doses). Mice were analysed 24 hour after the last injection. 5FU (250mg/kg) was injected i.v., and mice were analysed accordingly. For HSPC mobilization, mice received 2 (day 1), 4 (day 2), or 8 (day 4) consecutive injections of Filgrastim (Amgen) (125 µg/Kg twice a day s.c.) or saline.

Induction of *Cre^{ERTM}*-mediated recombination and iDTR mediated cell depletion

Male mice older than 8 weeks were injected with 1mg tamoxifen (Sigma) i.p. twice a day for five consecutive days as previously described[38]. For diphtheria toxin (DT) mediated cell

depletion, 100μg/kg of DT (Sigma) were injected i.p. 2 days after the last tamoxifen injection.

LTC-IC assay

To determine long-term culture-initiating cell (LTC-IC) numbers, serial dilutions of BMNC were plated on single-well stromal cultures; 4 weeks later each individual well was assayed for the presence of CFU-C as described[48]. BM HSC frequencies were estimated by the Newton-Raphson method of maximum likelihood and Poisson statistics as the reciprocal of the number of test cells that yielded a 37% negative response. LTC-IC frequencies and statistical significance were determined by using the ELDA software (http://bioinf.wehi.edu.au/software/elda/).

Competitive reconstitution

Competitive repopulation assays were performed using the CD45.1/CD45.2 congenic system. Equivalent volumes of BM cells harvested from NG2-*cre*[ERTM]/iDTR or Control mice (CD45.2) were transplanted into lethally irradiated (12Gy) CD45.1 recipients with 0.3×10^6 competitor CD45.1 cells. CD45.1/CD45.2 chimerism of recipients' blood was analysed up to 4 months after transplantation.

Computational modelling of HSC localization

Refer to Supplementary Fig. 4. The computational simulation was performed with MATLAB software.

Statistics

All data are represented as mean ± SEM. Comparisons between two samples were done using the unpaired Student's *t* tests. One-way ANOVA analyses followed by Tukey's multiple comparison tests were used for multiple group comparisons. Two-sample Kolmogorov-Smirnov tests were used for comparisons of distribution patterns. Statistical analyses were performed with Graph Pad Prism 6 or MATLAB software. * P <0.05, **P<0.01, ***P<0.001.

Supplementary Material

Refer to Web version on PubMed Central for supplementary material.

Acknowledgements

References

1. Orkin SH, Zon LI. Hematopoiesis: an evolving paradigm for stem cell biology. Cell. 2008; 132:631–644. [PubMed: 18295580]

2. Li L, Clevers H. Coexistence of quiescent and active adult stem cells in mammals. Science. 2010; 327:542–545. [PubMed: 20110496]

3. Hsu YC, Pasolli HA, Fuchs E. Dynamics between stem cells, niche, and progeny in the hair follicle. Cell. 2011; 144:92–105. [PubMed: 21215372]

4. Orford KW, Scadden DT. Deconstructing stem cell self-renewal: genetic insights into cell-cycle regulation. Nat Rev Genet. 2008; 9:115–128. [PubMed: 18202695]

5. Cheng T, et al. Hematopoietic stem cell quiescence maintained by p21cip1/waf1. Science. 2000; 287:1804–1808. [PubMed: 10710306]

6. Ito K, et al. PML targeting eradicates quiescent leukaemia-initiating cells. Nature. 2008; 453:1072–1078. [PubMed: 18469801]

7. Essers MA, et al. IFNalpha activates dormant haematopoietic stem cells in vivo. Nature. 2009; 458:904–908. [PubMed: 19212321]

8. Sato T, et al. Interferon regulatory factor-2 protects quiescent hematopoietic stem cells from type I interferon-dependent exhaustion. Nat Med. 2009; 15:696–700. [PubMed: 19483695]

9. Passegue E, Wagers AJ, Giuriato S, Anderson WC, Weissman IL. Global analysis of proliferation and cell cycle gene expression in the regulation of hematopoietic stem and progenitor cell fates. The Journal of experimental medicine. 2005; 202:1599–1611. [PubMed: 16330818]

10. Wilson A, et al. Hematopoietic stem cells reversibly switch from dormancy to self-renewal during homeostasis and repair. Cell. 2008; 135:1118–1129. [PubMed: 19062086]

11. Baldridge MT, King KY, Boles NC, Weksberg DC, Goodell MA. Quiescent haematopoietic stem cells are activated by IFN-gamma in response to chronic infection. Nature. 2010; 465:793–797. [PubMed: 20535209]

12. Zhang J, et al. Identification of the haematopoietic stem cell niche and control of the niche size. Nature. 2003; 425:836–841. [PubMed: 14574412]

13. Calvi LM, et al. Osteoblastic cells regulate the haematopoietic stem cell niche. Nature. 2003; 425:841–846. [PubMed: 14574413]

14. Sugimura R, et al. Noncanonical Wnt signaling maintains hematopoietic stem cells in the niche. Cell. 2012; 150:351–365. [PubMed: 22817897]

15. Arai F, et al. Tie2/angiopoietin-1 signaling regulates hematopoietic stem cell quiescence in the bone marrow niche. Cell. 2004; 118:149–161. [PubMed: 15260986]

16. Nilsson SK, et al. Osteopontin, a key component of the hematopoietic stem cell niche and regulator of primitive hematopoietic progenitor cells. Blood. 2005; 106:1232–1239. [PubMed: 15845900]

17. Stier S, et al. Osteopontin is a hematopoietic stem cell niche component that negatively regulates stem cell pool size. J Exp Med. 2005; 201:1781–1791. [PubMed: 15928197]

18. Kiel MJ, Yilmaz OH, Iwashita T, Terhorst C, Morrison SJ. SLAM family receptors distinguish hematopoietic stem and progenitor cells and reveal endothelial niches for stem cells. Cell. 2005; 121:1109–1121. [PubMed: 15989959]

19. Sugiyama T, Kohara H, Noda M, Nagasawa T. Maintenance of the hematopoietic stem cell pool by CXCL12-CXCR4 chemokine signaling in bone marrow stromal cell niches. Immunity. 2006; 25:977–988. [PubMed: 17174120]

20. Omatsu Y, et al. The essential functions of adipo-osteogenic progenitors as the hematopoietic stem and progenitor cell niche. Immunity. 2010; 33:387–399. [PubMed: 20850355]

21. Mendez-Ferrer S, et al. Mesenchymal and haematopoietic stem cells form a unique bone marrow niche. Nature. 2010; 466:829–834. [PubMed: 20703299]

22. Ding L, Saunders TL, Enikolopov G, Morrison SJ. Endothelial and perivascular cells maintain haematopoietic stem cells. Nature. 2012; 481:457–462. [PubMed: 22281595]

23. Ema H, Suda T. Two anatomically distinct niches regulate stem cell activity. Blood. 2012; 120:2174–2181. [PubMed: 22786878]

24. Hooper AT, et al. Engraftment and reconstitution of hematopoiesis is dependent on VEGFR2-mediated regeneration of sinusoidal endothelial cells. Cell stem cell. 2009; 4:263–274. [PubMed: 19265665]

25. Nombela-Arrieta C, et al. Quantitative imaging of haematopoietic stem and progenitor cell localization and hypoxic status in the bone marrow microenvironment. Nat Cell Biol. 2013; 15:533–543. [PubMed: 23624405]

26. Li XM, Hu Z, Jorgenson ML, Slayton WB. High levels of acetylated low-density lipoprotein uptake and low tyrosine kinase with immunoglobulin and epidermal growth factor homology domains-2 (Tie2) promoter activity distinguish sinusoids from other vessel types in murine bone marrow. Circulation. 2009; 120:1910–1918. [PubMed: 19858415]

27. Shen Z, Lu Z, Chhatbar PY, O'Herron P, Kara P. An artery-specific fluorescent dye for studying neurovascular coupling. Nat Methods. 2012; 9:273–276. [PubMed: 22266543]

28. Takaku T, et al. Hematopoiesis in 3 dimensions: human and murine bone marrow architecture visualized by confocal microscopy. Blood. 2010; 116:e41–e55. [PubMed: 20647571]

29. Naveiras O, et al. Bone-marrow adipocytes as negative regulators of the haematopoietic microenvironment. Nature. 2009; 460:259–263. [PubMed: 19516257]

30. Katayama Y, et al. Signals from the sympathetic nervous system regulate hematopoietic stem cell egress from bone marrow. Cell. 2006; 124:407–421. [PubMed: 16439213]

31. Mendez-Ferrer S, Lucas D, Battista M, Frenette PS. Haematopoietic stem cell release is regulated by circadian oscillations. Nature. 2008; 452:442–447. [PubMed: 18256599]

32. Yamazaki S, et al. Nonmyelinating Schwann cells maintain hematopoietic stem cell hibernation in the bone marrow niche. Cell. 2011; 147:1146–1158. [PubMed: 22118468]

33. Bhattacharya D, et al. Niche recycling through division-independent egress of hematopoietic stem cells. J Exp Med. 2009; 206:2837–2850. [PubMed: 19887396]

34. Kalajzic Z, et al. Directing the expression of a green fluorescent protein transgene in differentiated osteoblasts: comparison between rat type I collagen and rat osteocalcin promoters. Bone. 2002; 31:654–660. [PubMed: 12531558]

35. Liu F, et al. Csf3r mutations in mice confer a strong clonal HSC advantage via activation of Stat5. J Clin Invest. 2008; 118:946–955. [PubMed: 18292815]

36. Greenbaum AM, Link DC. Mechanisms of G-CSF-mediated hematopoietic stem and progenitor mobilization. Leukemia. 2011; 25:211–217. [PubMed: 21079612]

37. Birbrair A, et al. Skeletal muscle pericyte subtypes differ in their differentiation potential. Stem Cell Res. 2012; 10:67–84. [PubMed: 23128780]

38. Zhu X, et al. Age-dependent fate and lineage restriction of single NG2 cells. Development. 2011; 138:745–753. [PubMed: 21266410]

39. Chi JT, et al. Endothelial cell diversity revealed by global expression profiling. Proc Natl Acad Sci U S A. 2003; 100:10623–10628. [PubMed: 12963823]

40. Frenette PS, Pinho S, Lucas D, Scheiermann C. Mesenchymal Stem Cell: Keystone of the Hematopoietic Stem Cell Niche and a Stepping-Stone for Regenerative Medicine. Annual review of immunology. 2013

41. Greenbaum A, et al. CXCL12 in early mesenchymal progenitors is required for haematopoietic stem-cell maintenance. Nature. 2013; 495:227–230. [PubMed: 23434756]

42. Ding L, Morrison SJ. Haematopoietic stem cells and early lymphoid progenitors occupy distinct bone marrow niches. Nature. 2013; 495:231–235. [PubMed: 23434755]

43. Sipkins DA, et al. In vivo imaging of specialized bone marrow endothelial microdomains for tumour engraftment. Nature. 2005; 435:969–973. [PubMed: 15959517]

44. Winkler IG, et al. Vascular niche E-selectin regulates hematopoietic stem cell dormancy, self renewal and chemoresistance. Nat Med. 2012

45. Mignone JL, Kukekov V, Chiang AS, Steindler D, Enikolopov G. Neural stem and progenitor cells in nestin-GFP transgenic mice. The Journal of comparative neurology. 2004; 469:311–324. [PubMed: 14730584]

References (ON LINE ONLY)

46. Kawamoto T. Use of a new adhesive film for the preparation of multi-purpose fresh-frozen sections from hard tissues, whole-animals, insects and plants. Arch Histol Cytol. 2003; 66:123–143. [PubMed: 12846553]

47. Chiang EY, Hidalgo A, Chang J, Frenette PS. Imaging receptor microdomains on leukocyte subsets in live mice. Nat Methods. 2007; 4:219–222. [PubMed: 17322889]

48. Miller CL, Dykstra B, Eaves CJ. Characterization of mouse hematopoietic stem and progenitor cells. Curr Protoc Immunol. 2008; Chapter 22(Unit 22B):22.
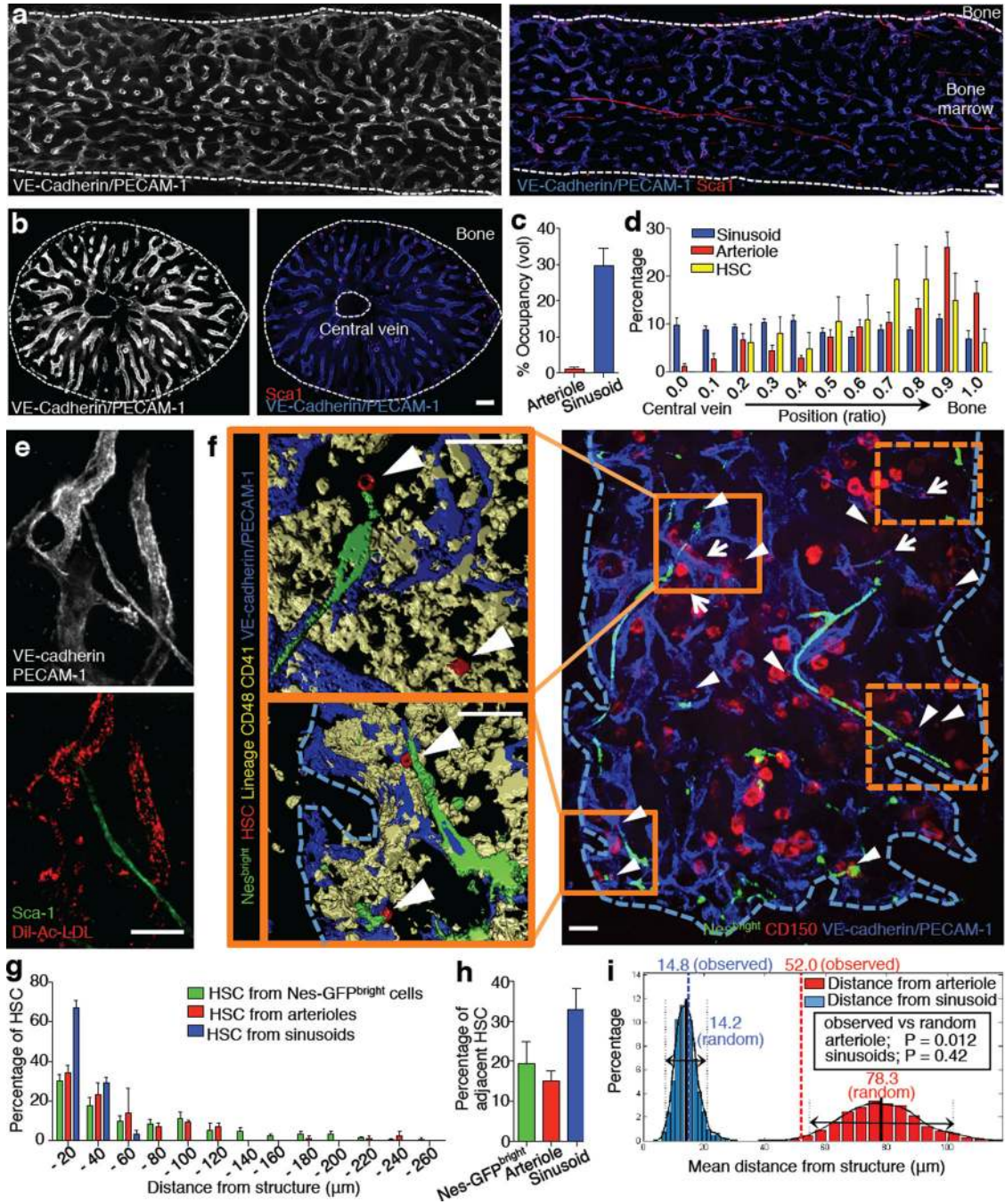
Figure 1. Spatial relationships between HSCs and the bone marrow vasculature
a,b, Longitudinally (**a**) and transverse-shaved (**b**) whole-mount images of the mouse femoral BM stained with anti-PECAM-1, anti-VE-cadherin and anti-Sca-1 antibodies. Scale bar: 100 μm. **c,** BM volumes occupied by arterioles or sinusoids. n = 6 areas from 3 mice. **d,** Distribution of sinusoids, arterioles and HSCs in the femoral BM. n = 6 mice. **e,** Whole-mount images of sternum stained with anti-VE-cadherin, anti-PECAM-1, anti-Sca-1 antibodies and Dil-Ac-LDL. Scale bar: 50 μm. **f,** Illustrative example of whole-mount sternal BM with 3D reconstructed images. Dashed squares are shown in Extended Data Fig.

3b. Arrowheads denote HSCs, arrows show CD150$^+$ Lin/CD48/CD41$^+$ cells. Scale bar: 50 μm. **g,h,** Distances between HSCs and Nes-GFP^{bright} cells (n = 98 HSCs from 5 mice), arterioles or sinusoids (n = 119 HSCs from 5 mice) (**g**) and percentages of adjacent HSCs (distance = 0) (**h**) in the sternal BM. **i,** Probability distributions of mean distances from simulations of randomly positioned HSCs on maps of sternal BM in relation to sinusoids (blue) or arterioles (red). Mean distances observed *in situ* (dashed) are shown in relation to the grand mean ± 2 s.d. (solid and dotted lines).
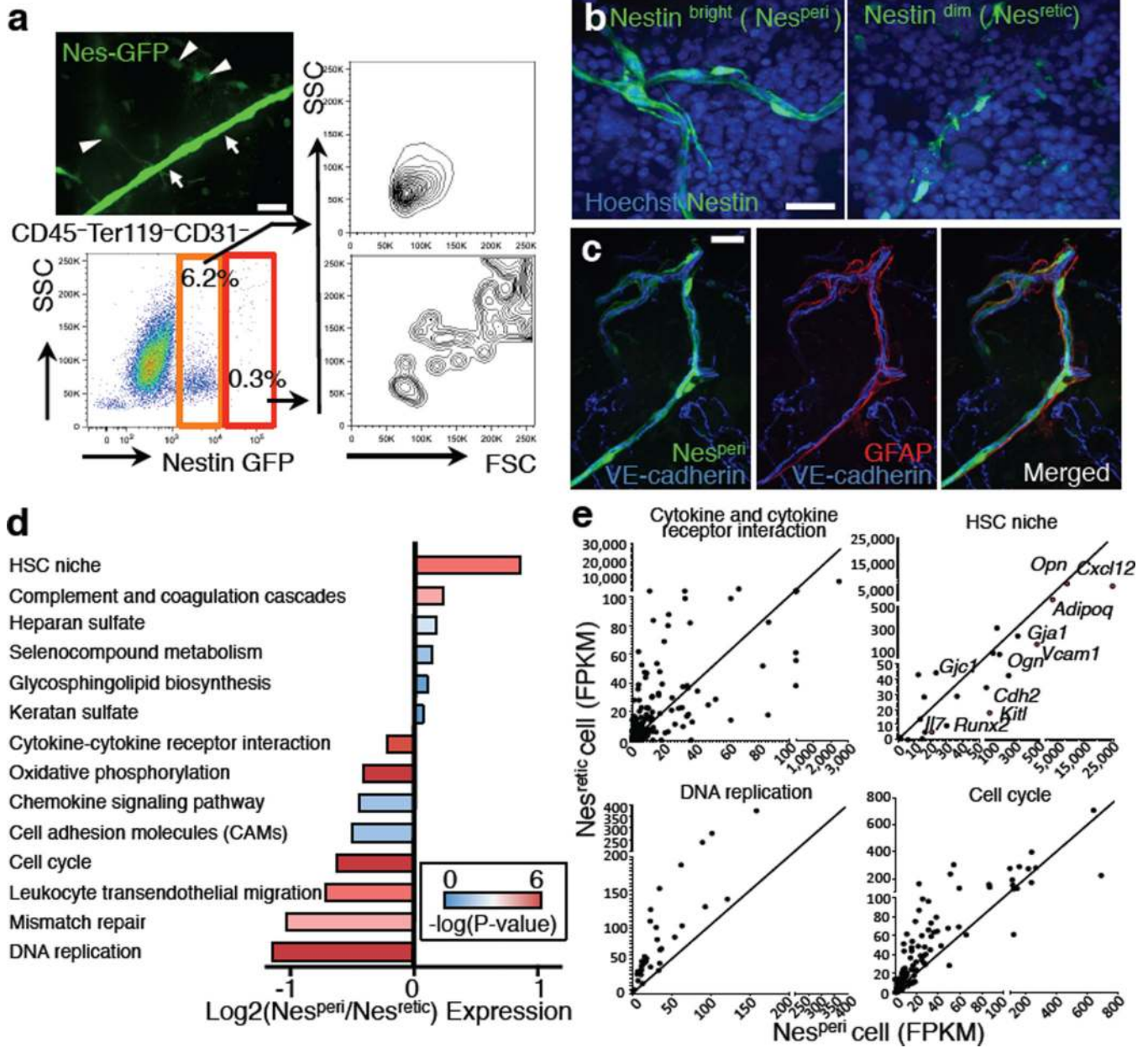
Figure 2. Nestin⁺ cell subsets define distinct vascular structure

a, A whole-mount image of sternal BM with Nes-GFP^bright (arrows) and Nes-GFP^dim cells (arrowheads) and FACS analysis of BM stromal cells from Nes-GFP mice. Data were reproducible in at least 5 mice. **b,c,** Whole-mount images of sternum from Nes-GFP mice stained with anti-GFP and Hoechst 33342 (**b**) or anti-GFAP antibody (**c**). **d,e,** RNA-seq analysis of Nes^retic and Nes^peri cells. **d,** Differentially expressed pathways. Mean of log fold change of Nes^peri/Nes^retic expression was plotted for each pathway with colour-coded P-values. **e,** Dot plots showing gene expression levels in FPKM for representative pathways and functional groups.
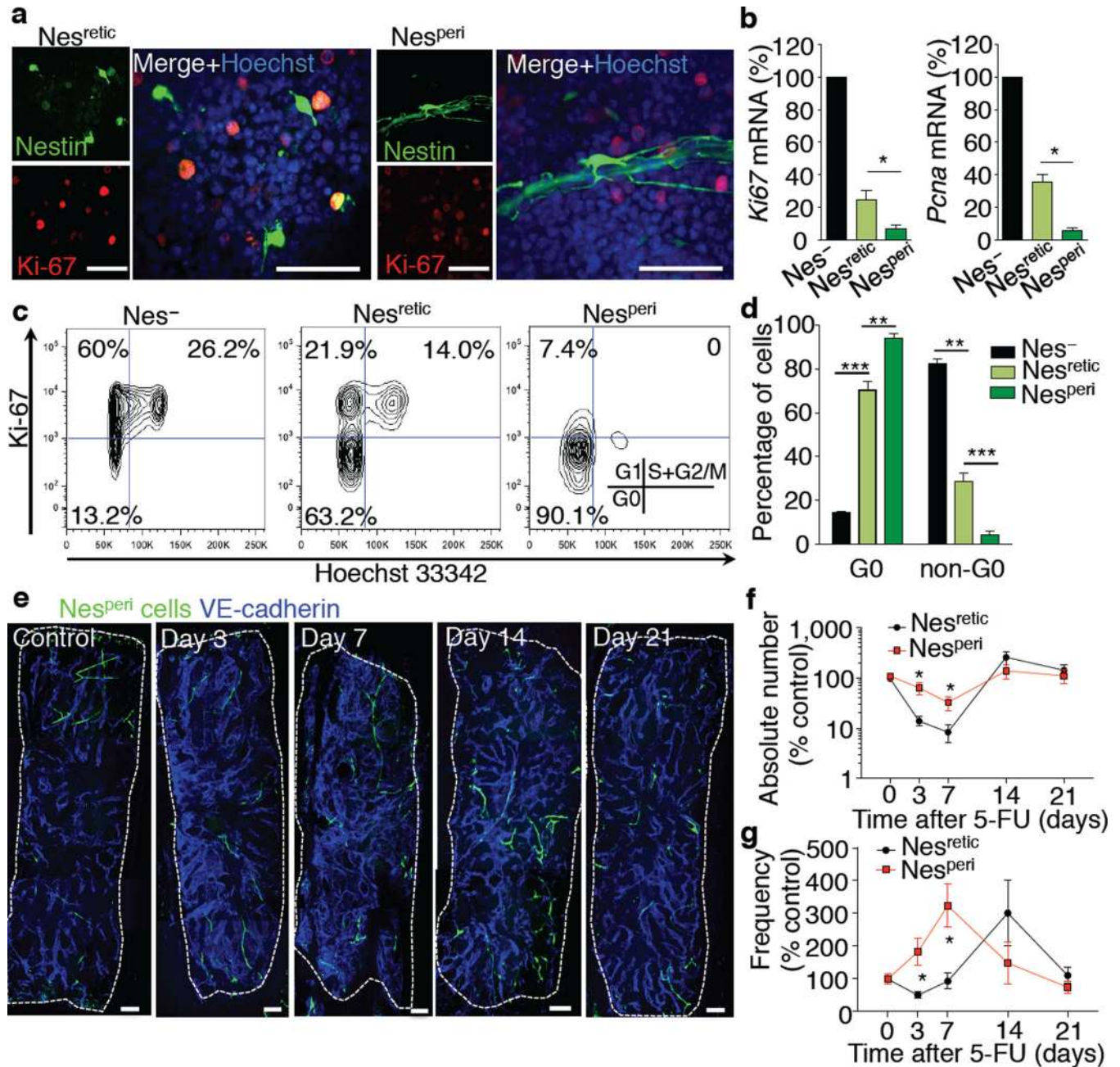
Figure 3. Quiescent arteriolar niche cells are protected from myeloablation

a, Whole-mount immunostaining with anti-Ki-67 antibody of sterna from Nes-GFP mice. Scale bar: 50 μm. **b,** Q-PCR analyses of Nes[peri], Nes[retic] and CD45^{−} Ter119^{−} CD31^{−} Nes-GFP^{−} stromal cells. n = 5 independent experiments. **c,d,** Cell cycle analyses by FACS using anti-Ki-67 and Hoechst 33342 staining. Representative plots (**c**) and quantification (**d**). n = 3 mice per group. **e–g,** Whole mount images of sternal BM (**e**) and the kinetics of absolute numbers (**f**) and frequencies (**g**) of Nes[peri] and Nes[retic] cells in the long-bone BM analysed by FACS after 5FU treatment. n = 10, 9, 9, 5, 6 mice per time point. Scale bar: 100 μm.
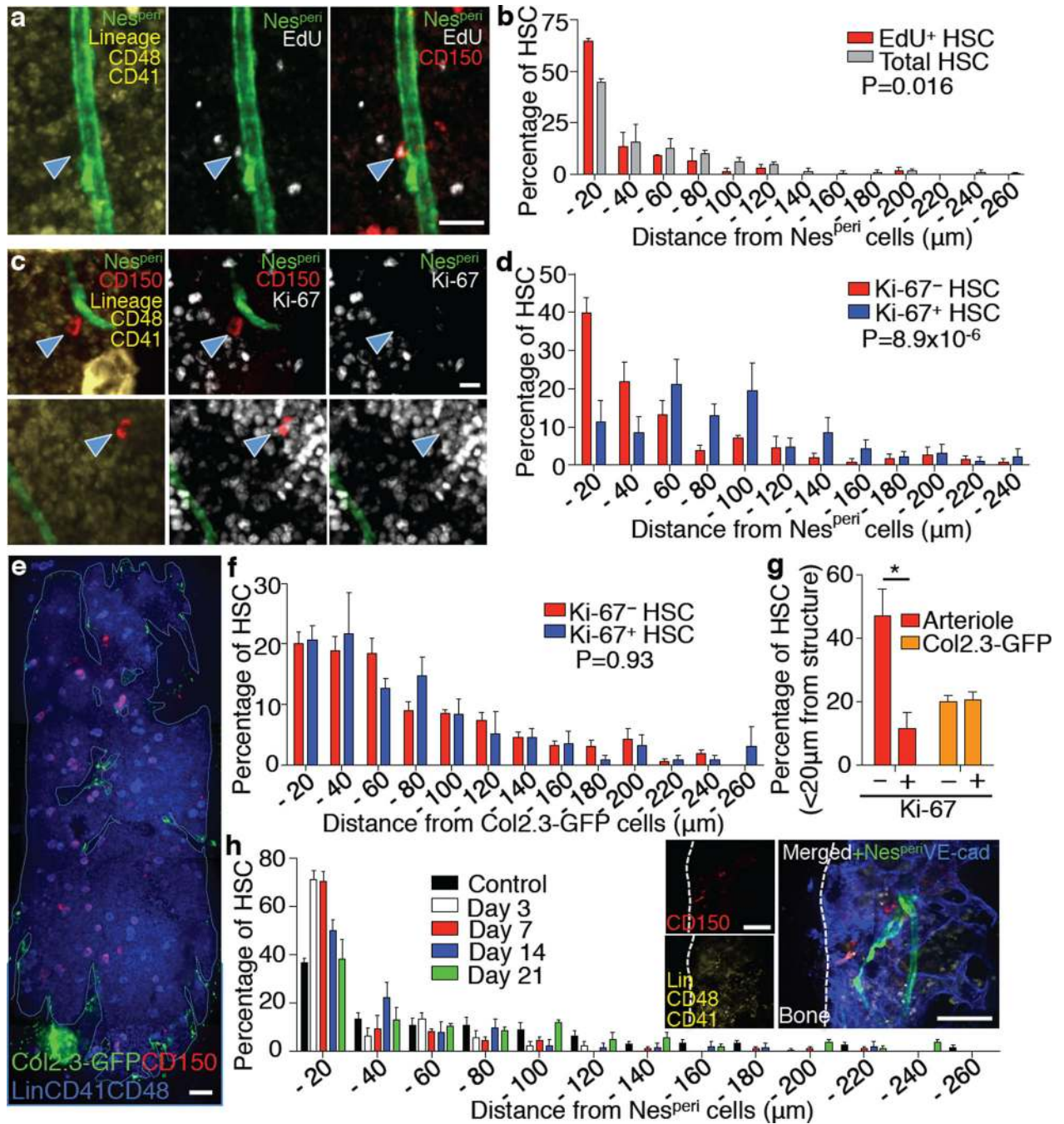
Figure 4. Spatial relationship between arterioles and quiescent HSCs
a,b, Localization of dormant HSCs accessed by long-term label retention with EdU. Representative images (**a**) and distribution of total and EdU+ CD150+ CD48− CD41− Lineage− HSCs in femoral BM sections (**b**). n = 144, 52 HSCs from 3 mice. Two-sample Kolmogorov-Smirnov test; P = 0.016. Scale bar: 25 μm. **c,d,** Localization of Ki-67− and Ki-67+ HSCs in the sternal BM. Ki-67− / Ki-67+: 39.7±3.9% / 11.4±5.6% in 0–20μm proximity, 21.5±5.3% / 47.9±6.5% > 80μm distance. Representative images (**c**) and distances from Nes^peri cells (**d**). n = 116, 64 HSCs from 7 mice. Two-sample Kolmogorov-

Smirnov test; P = 8.9×10^{-6}. Scale bar: 10 μm. **e–g,** Localization of HSCs in relation to osteoblasts. **e,** Whole-mount images of sternum from Col2.3-GFP mice with HSC staining. Scale bar: 100 μm. **f,** Distances of Ki-67$^-$ and Ki-67$^+$ HSCs from Col2.3-GFP cells. n = 80, 41 HSCs from 3 mice. Two-sample Kolmogorov-Smirnov test; P = 0.93. **g,** Percentage of Ki-67$^-$ and Ki-67$^+$ HSCs located within 20μm distance from arterioles or Col2.3-GFP cells. n = 7, 3 mice per group. **h,** Localization of HSCs relative to Nes^{peri} cells after 5FU treatment. Inset shows a representative image of sternal BM on day 7. n = 98, 39, 70, 55, 112 HSCs from 5, 9, 7, 4, 4 mice per group. Two-sample Kolmogorov-Smirnov test; Day 3 P =2.8×10^{-4}, Day 7 P =1.0×10^{-4}, Day 14 P =0.0013, Day 21 P =0.23 compared to control. Scale bar: 50 μm.
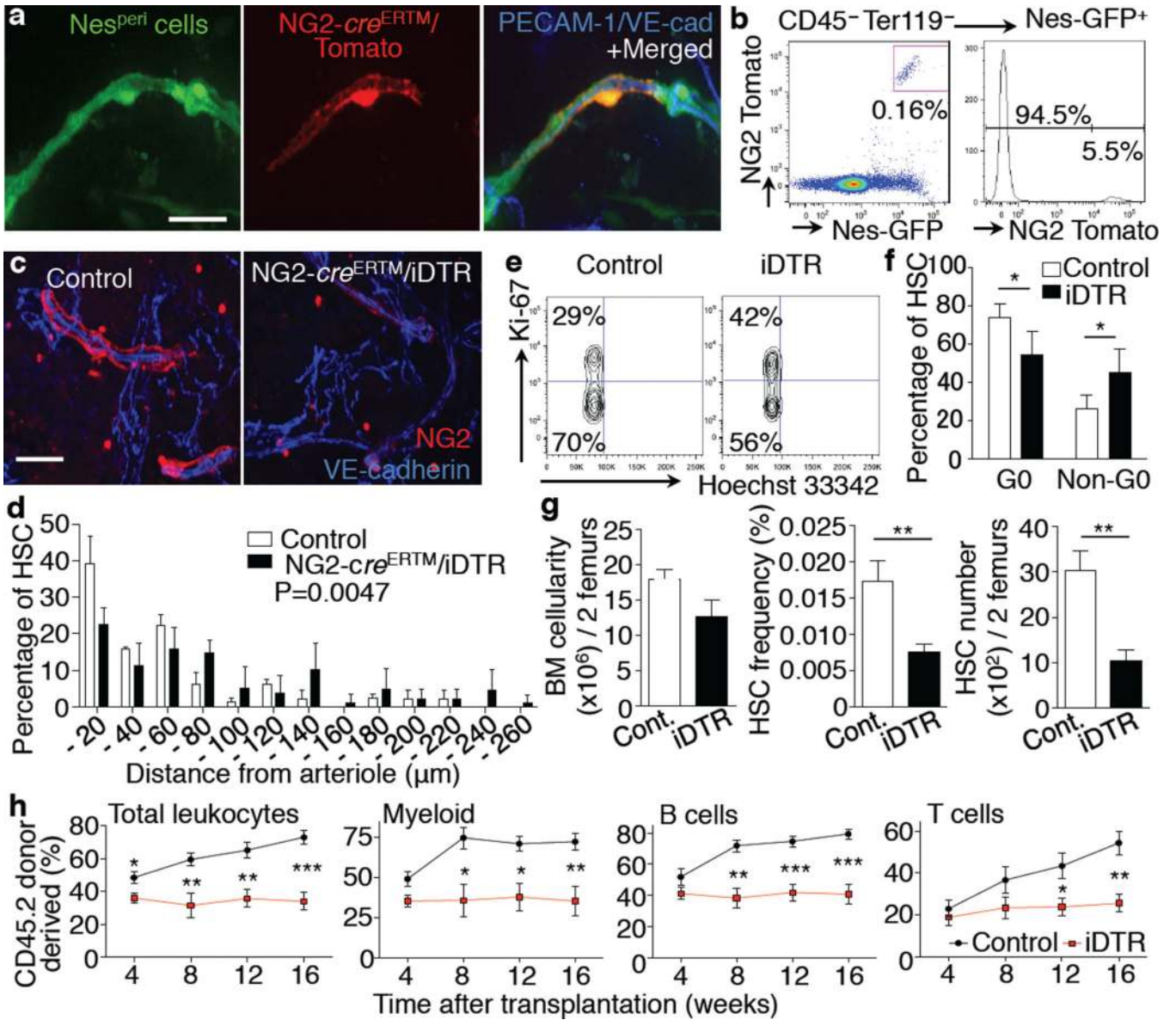
Figure 5. NG2+ periarteriolar cells are an essential constituent of the HSC niche promoting HSC quiescence

a,b, Whole-mount images of sternal BM (**a**) and FACS analysis of femoral BM (**b**) from NG2-cre[ERTM] / loxp-Tomato / Nes-GFP Tg mice. Representative data of 4 mice. **c–h,** Analysis of HSCs after specific deletion of NG2+ cells using NG2-cre[ERTM]/iDTR mice. **c,** Whole-mount immunostaining of sternum with anti-NG2 antibody. Representative images of 5 mice per group. **d,** HSC localization relative to arterioles in the sternal BM. n = 69, 71 HSCs from 3, 4 mice per group. Two-sample Kolmogorov-Smirnov test; P = 0.0047. **e,f,** Cell cycle analysis of HSCs using Ki-67 and Hoechst 33342 staining. Representative plots (CD150+ CD48− Sca-1+ c-kit+ Lineage− gated) (**e**) and quantifications (**f**). n = 5 mice per group. **g,** BM cellularity, frequency and number of HSCs in the BM. n = 6 mice per group.

h, Quantification of long-term reconstituting HSCs by competitive reconstitution assays. n = 6, 9 mice per group. Scale bar: 25 μm.